THE JOURNAL OF PHYSICAL CHEMISTRY B

ARTICLE

pubs.acs.org/JPCB

Interaction of 7-Nitrobenz-2-oxa-1,3-diazol-4-yl-Labeled Fatty Amines with 1-Palmitoyl, 2-Oleoyl-*sn*-glycero-3-phosphocholine Bilayers: A Molecular Dynamics Study

Hugo A. L. Filipe,[†] Maria João Moreno,[†,‡] and Luís M. S. Loura*[,†,§]

[†]Centro de Química de Coimbra, Universidade de Coimbra, Largo D. Dinis, Rua Larga, 3004-535 Coimbra, Portugal

[‡]Departamento de Química, Faculdade de Ciências e Tecnologia, Universidade de Coimbra, Largo D. Dinis, Rua Larga, 3004-535 Coimbra, Portugal

[§]Faculdade de Farmácia, Universidade de Coimbra, Pólo das Ciências da Saúde, Azinhaga de Santa Comba, 3000-548 Coimbra, Portugal

Supporting Information

ABSTRACT: A complete homologous series of fluorescent 7-nitrobenz-2-oxa-1,3-diazol-4-yl (NBD)-labeled fatty amines of varying alkyl chain length, NBD-C_n, inserted in 1-palmitoyl, 2-oleoyl-*sn*-glycero-3-phosphocholine (POPC) bilayers, was studied using atomistic molecular dynamics (MD) simulations. For all amphiphiles, the NBD fluorophore locates near the glycerol backbone/carbonyl region of POPC and establishes stable hydrogen bonding with POPC ester oxygen atoms. Small differences observed in the transverse location of the fluorophore correlate with other calculated parameters and with small discrepancies recently measured in the photophysical properties of the molecules. The longer-chained NBD-C_n amphiphiles show significant mass density near the bilayer midplane, and the chains of these derivatives interdigitate to some extent the opposite bilayer leaflet. This phenomenon leads to a slower lateral diffusion for the longer-chained derivatives ($n > 12$). Effects of these amphiphiles on the structure and dynamics of the host lipid were found to be relatively mild, in comparison with acyl-chain-labeled NBD probes. The molecular details obtained by this work allow the rationalization of the nonmonotonic behavior, recently obtained experimentally, for the photophysical parameters of the amphiphiles and the kinetic and thermodynamic parameters for their interaction with the POPC membranes.

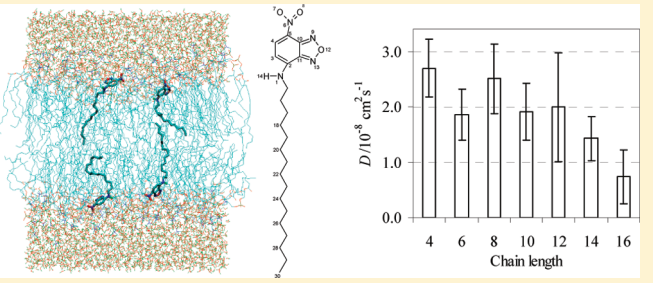

INTRODUCTION

The interaction of amphiphilic molecules with lipid bilayers is a very important step that determines their location inside the cells and the rate of permeation across the different hydrophobic barriers in the cell or organism. Molecules with pharmacological or biological activity are usually amphiphilic due to their need to cross different cell membranes before they reach the target site and become active molecules. The establishment of quantitative relationships between the amphiphile structure and its rate of permeation through biomembranes is therefore an important tool in the rational development of new drugs, and this has been addressed by us[1−5] and other authors (see, e.g., refs 6−14).

In addition to applications in the enhancement of drug bioavailability, the interaction between amphiphilic molecules with different lengths in the alkyl or acyl chain and lipid bilayers is also of fundamental importance for the understanding of the consequences of protein modification by acylation.[8,11,15,16] This is a prevalent cell regulation process where the association between the protein and a given membrane is enhanced, leading to an increased activity via its local concentration or inhibition by sequestration.[16,17]

In the last years, this research team has been characterizing in detail the interaction of amphiphiles with serum proteins and lipid bilayers regarding both equilibrium and kinetic parameters.[1−5,18] More recently, the homologous series of fatty amines labeled with the fluorescent moiety 7-nitrobenz-2-oxa-1,3-diazol-4-yl (NBD[19]) has been studied, and the effect of the length of the alkyl chain on their solubility in aqueous media, binding to serum proteins, and partitioning to lipid bilayers[1,20] has been characterized. The results obtained revealed nonmonotonic behavior along the homologous series. This has prompted us to characterize their interaction with lipid bilayers using molecular dynamics (MD) simulations, so as to gain molecular detail on the interactions established.

The interaction of fluorescent molecules with lipid bilayers is also a very important tool in the characterization of the lipid bilayer itself.[21] For that purpose, in addition to equilibrium and kinetic parameters for the interaction, it is necessary to know the

Received: April 15, 2011
Revised: July 7, 2011
Published: July 12, 2011

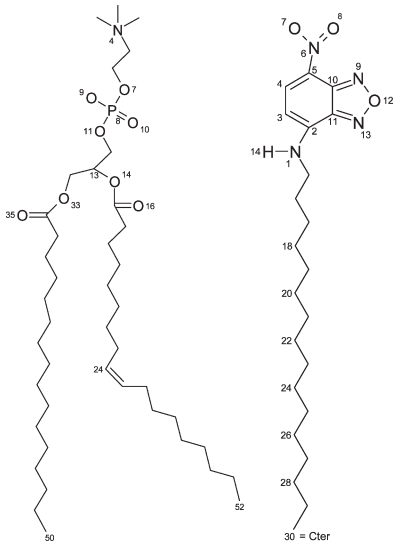

Figure 1. Structures of POPC (left) and NBD-C_{16} (right), showing the atom numbering as used throughout the text.

location of the amphiphile in the membrane and its effects on the properties of the system under study. MD simulations are a priceless tool for this purpose, as all of the details of the interaction may be established, and have been used to obtain detailed atomic-scale information on phospholipid bilayers (e.g., see ref 22 for a review). They are suitable for the calculation of a variety of properties of fluorescent probes in the bilayer, as well as their effect on the organization of the latter. This has been demonstrated recently for several different fluorophores,[23−35] including NBD-labeled lipids by ourselves.[23,27,30] In this report, we have undertaken the systematic characterization of the association of NBD-C_n amphiphiles (Figure 1) with 1-palmitoyl, 2-oleoyl-*sn*-glycero-3-phosphocholine (POPC) bilayers using atomistic MD simulations, to obtain information regarding the effects of the alkyl chain length on the location, orientation, and dynamics of the polar group in the bilayer and thus complement the experimental work recently carried out on the association of these molecules with serum proteins and POPC vesicles.[1,20]

SIMULATION DETAILS

MD simulations and analysis of trajectories was carried out using the GROMACS 3.2 package.[36,37] The simple point charge (SPC) water model was used.[38] The topology of the POPC molecule (using a united-atom description for CH, CH_2, and CH_3 groups, based on the parameters presented by Berger et al.[39] for 1,2-dipalmitoyl-*sn*-glycero-3-phosphatidylcholine (DPPC)) and the coordinate file of a POPC bilayer were obtained from Dr. Peter Tieleman's group webpage (http://moose.bio.ucalgary.ca/index.php?page=Structures_and_Topologies).[34] One POPC molecule from the downloaded POPC bilayer coordinate file was used to build a fully hydrated (3902 water molecules) 128 lipid bilayer using GROMACS model setup programs. For the CH_2 and CH_3 groups of NBD-C_n molecules, parameters were based on those of the phospholipid. For the NBD fluorophore, a preliminary topology was obtained using the PRODRG server.[40] Equilibrium bond lengths, angles, and dihedrals were obtained through energy minimization carried out with the Gamess-US package.[41,42] Other parameters were taken from the optimized potentials for liquid simulations (OPLS) all-atom forcefield.[43] All bonding and nonbonding parameters are shown in the Supporting Information file of ref 23. Partial charges of the NBD group atoms were derived from ab initio quantum mechanical calculations[44] using Gamess-US, and their values are given in Table 1 of ref 30. Figure 1 shows structures and numbering of relevant atoms of the POPC and NBD-C_{16} molecules. Bilayers containing 2 and 4 NBD-C_n molecules (1 and 2 in each leaflet, respectively) were obtained by randomly inserting probe molecules inside the POPC bilayer without replacement of phospholipids. In all systems, unfavorable atomic contacts were removed by steepest descent energy minimization. For each system, a short (100 ps) MD run was then carried out using a 1 fs integration step, followed by a 100 ns run using a 4 fs integration step. The use of this time step was made possible by constraining bond lengths and angles to their equilibrium values, using the SETTLE algorithm[45] for water and the LINCS algorithm[46] for all other bonds (see also discussion in refs 47 and 48). All simulations were carried out under constant number of particles, pressure (1 bar), and temperature (298.15 K) and with periodic boundary conditions. Pressure and temperature control was carried out using the weak-coupling Berendsen schemes,[49] with coupling times of 1.0 and 0.1 ps, respectively. Semi-isotropic pressure coupling was used. van der Waals and Coulomb interactions were cut off at 1.0 nm, whereas for long-range electrostatics the particle-mesh Ewald treatment[50] was applied. The first 20 ns of each simulation were used for equilibration, and the remaining 80 ns were used for analysis. Error estimates for time averages of correlated data were computed using the block method as described by Flyvbjerg and Petersen.[51] Unless stated otherwise, and for the purpose of a better statistical description of the amphiphile properties, the analyzed results here reported concern the 4 NBD-C_n systems, as no significant differences in behavior were observed in the 2 NBD-C_n simulations.

Table 1. Average Area per Lipid and Average P−P Distance Obtained from MD Simulations

system	area per lipid, a/nm^2	P−P distance/nm
POPC	0.625 ± 0.015	3.80 ± 0.11
POPC/NBD-C_4	0.628 ± 0.020	3.82 ± 0.13
POPC/NBD-C_6	0.644 ± 0.021	3.74 ± 0.12
POPC/NBD-C_8	0.625 ± 0.020	3.82 ± 0.12
POPC/NBD-C_{10}	0.644 ± 0.020	3.76 ± 0.12
POPC/NBD-C_{12}	0.639 ± 0.020	3.78 ± 0.13
POPC/NBD-C_{14}	0.625 ± 0.021	3.85 ± 0.12
POPC/NBD-C_{16}	0.633 ± 0.020	3.82 ± 0.13

RESULTS AND DISCUSSION

Area per Lipid. The instant area per lipid molecule, a, was calculated as the instant box area divided by the number of lipid molecules in each monolayer (64), for both pure POPC bilayers and 4 NBD-C_n/128 POPC bilayers. The time variation of the area per lipid is a common indicator of the equilibration of the bilayer, whereas its average value is often used to assess the adequacy of the simulation methodology, due to its sensitiveness to simulation details.[48]

Figure S1 in the Supporting Information (SI) file shows that, whereas variations of this parameter's value are large in the initial stages of the simulations, they are considerably reduced for $t >$ 20 ns. In an attempt to clarify this situation, the cumulative

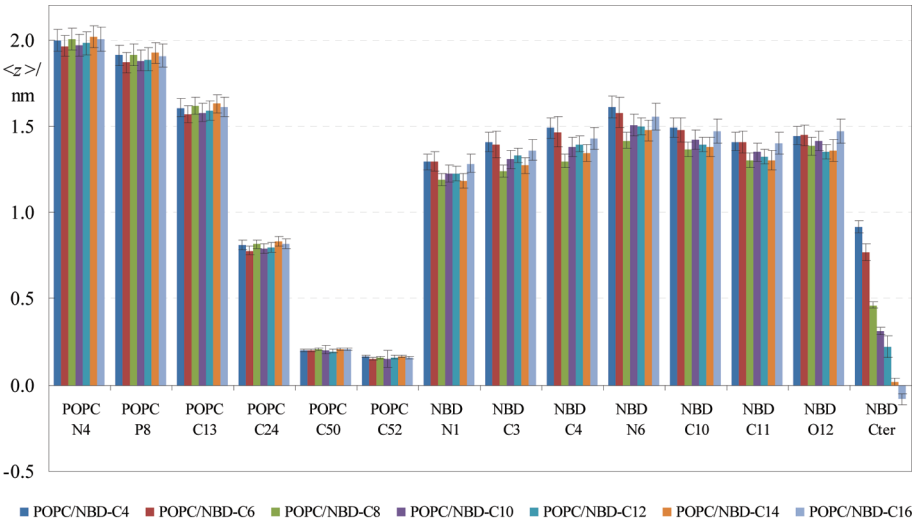

Figure 2. Average transverse position <*z*> of specific atoms in the POPC/NBD-C_n systems. See Figure 1 for atom numbering. Cter represents the methyl group at the end of the fatty amine chain.

moving averages of *a* in the [20 ns, *t*] interval are represented in Figure S2 of the SI. Although some systems appear to be still slowly evolving near the end of the simulation (possibly NBD-C_{12} and NBD-C_{16}), in all cases the variation of this cumulative average is ≤2% (or 0.013 nm^2) for $t > 40$ ns and less than 0.5% (or 0.0030 nm^2) for $t > 80$ ns. This indicates that, even if those particular systems might not be completely equilibrated, they should be very close to equilibrium, validating the use of the last 80 ns of the full length simulations for analysis. As expected, the incorporation of two NBD-C_n molecules in each bilayer leaflet (keeping the number of POPC molecules constant) generally increases the area/lipid values. The average values of *a* for the simulations are shown in Table 1 and fall between $a = 0.625$ nm^2 for both POPC/NBD-C_8 and POPC/NBD-C_{14} (these values are in fact identical to that recovered for a pure POPC bilayer) and 0.644 nm^2 for POPC/NBD-C_6 and POPC/NBD-C_{10}. As shown in Table 1, nonmonotonic variations, not larger than the standard error, are observed. However, even at this point it should be stressed that these relatively slight variations correlate with several other observables obtained from this work, as well as previous experimental data, as discussed in detail below. The results for pure POPC agree with the experimental values of 0.65 nm^2 ($T = 298$ K),[52] 0.64 nm^2 ($T = 298$ K),[53] and 0.63 nm^2 ($T = 297$ K),[54] as well as with those obtained from MD simulations by Böckmann et al. ($T = 300$ K, $a = 0.655$ nm^2),[55] Mukhopadhyay et al. ($T = 298$ K, $a = 0.62$ nm^2),[56] Gurtovenko and Anwar ($T = 310$ K, $a = 0.65$ nm^2),[57] and Pandit et al. ($T = 303$ K, $a = 0.630$ nm^2).[58]

Bilayer Thickness and Position of Different Atoms. Figure 2 shows average transverse positions <*z*> for selected atoms along the POPC and NBD-C_n molecules. It should be noted that, in the course of the simulations, one amphiphile molecule in each of the 4 NBD-C_4, 4 NBD-C_6, and 4 NBD-C_8 simulations was observed to escape the bilayer into the water medium. In the 4 NBD-C_6 and 4 NBD-C_8 systems (not in the 4 NBD-C_4 system), these molecules returned to the bilayer during the course of the simulation run, essentially to the same transverse location as displayed by the three remaining molecules. In any case, these escaping molecules were omitted from the results here presented. The positions of the atoms of the NBD-fatty amines are consistent with the perpendicular orientation relative to the bilayer plane, with the NBD group near the glycerol backbone/upper acyl chain region (similar to the location of this fluorophore in 1-palmitoyl-2-[6-(7-nitrobenz-2-oxa-1,3-diazol-4-yl)aminohexanoyl]-*sn*-glycero-3-phosphocholine (C6-NBD-PC) and 1-palmitoyl-2-[12-(7-nitrobenz-2-oxa-1,3-diazol-4-yl)-aminododecanoyl]-*sn*-glycero-3-phosphocholine (C12-NBD-PC), determined by molecular simulation[30] and verified experimentally[59,60]) and the fatty-chain end methyl group, Cter, directed to the center of the bilayer.

From the average transverse position <*z*> of the POPC P atoms we can calculate the thickness of the bilayer as the distance between the average transverse locations of these atoms in opposing leaflets ($(P-P)_{dist}$; see Table 1). The results show a minimum $(P-P)_{dist} = 3.74 \pm 0.12$ nm for POPC/NBD-C_6 and a maximum $(P-P)_{dist} = 3.85 \pm 0.12$ nm for POPC/NBD-C_{14}, which correlate with maximal and minimal (respectively) area per lipid values in these systems; see Table 1. In fact, the variation of $(P-P)_{dist}$ with the amphiphile chain length is almost a mirror image of that of *a*, as could be expected, and similarly to the latter, the variations in $(P-P)_{dist}$ fall within the calculated standard errors.

To gain insight on the conformation of the hydrocarbon chain of the amphiphiles, the transverse distance between the NBD N1 and Cter atoms was calculated for each amphiphile. Figure 3 shows that this distance increases almost linearly with the chain length of the amphiphiles, with a slope of 0.083 nm/CH_2 group. This value is considerably smaller (because of *gauche* defects) than the limit for an all-*trans* chain of 0.127 nm[61] and is very similar to that observed for the *sn*-1 chain of POPC (not shown). From this result it may be inferred that the average angle between C−C bonds in the carbon chain (or the fraction of *gauche* defects along the chain) is similar for all amphiphiles. In any case, as shown in Figure 3, the average distances observed for $n \geq 12$ are somewhat smaller than expected from the trend established by the $n < 12$ values (with the slope of 0.091 nm/CH_2 shown in the figure). Additionally, the standard error associated with the average transverse N1−Cter distance increases with *n*. This effect was not observed for *z*(N1) (Figure 2). The shift in behavior between the shorter-chained ($n \leq 10$) and longer-chained ($n \geq 12$)

dx.doi.org/10.1021/jp203532c |*J. Phys. Chem. B* 2011, 115, 10109–10119

amphiphiles correlates with experimental observables previously measured by our group, such as the rate of translocation.[20]

Figure 4 shows a comparison between <z> of C13 of POPC and N6 of NBD-C_n (panel A) and between <z> of C24 of POPC (carbon 9 of the *sn*-2 chain) and the Cter of NBD-C_n (panel B). The results show that C13 of POPC and N6 of NBD are essentially positioned at the same depth in the bilayer for the shorter chain amphiphiles. For the longer chained amphiphiles, the NBD N6 atom presents a smaller <z>, and the deepest and most shallow transverse locations of this fluorophore atom are observed for NBD-C_8 and NBD-C_{16}, respectively. With the exception of these two values, variations of the NBD N6 <z> for $n \geq 8$ are of the order of the estimated errors. Even so, it should be pointed that these variations are mostly parallel to those of the area/lipid molecule a, with NBD-C_8 and NBD-C_{14} presenting both the deepest NBD transverse locations (Figures 2 and 4A) and smaller a values (Table 1). This can be understood taking into account that these analogues have the bulky NBD group located in a less crowded region of the bilayer, where it can be accommodated without pushing aside nearby POPC molecules. Probably for this reason, a values in these systems are essentially identical to that of unlabeled POPC bilayers (Table 1). This is at variance with the other NBD-C_n analogues, for which the fluorophore has a more shallow location, near the maximum of POPC mass density profile (see Figure 11 below).

On the other hand, as shown in panel B, as the fatty amine chain becomes longer, the average transverse location of the Cter group becomes increasingly deeper in the bilayer. Cter of NBD-C_4 and NBD-C_6 are located above the *sn*-2 *cis* double bond (which connects POPC C24 and POPC C25, the coordinates of the former also shown in the figure), whereas those of NBD-C_8, -C_{10}, -C_{12}, -C_{14}, and -C_{16} are located more internally.

Interestingly, <z>(Cter) = (-0.083 ± 0.032) nm for NBD-C_{16} is negative, indicating interdigitation of this amphiphile's chain and the POPC acyl chains in the opposing leaflet. This effect is not limited to this molecule, as for example <z>(Cter) = (0.020 ± 0.023) of NBD-C_{14} indicates an average transverse location in the bilayer midplane. The snapshot of Figure 5 (left panel) illustrates clear interdigitation for one of the represented molecules.

A possible way to quantify this phenomenon is to calculate the fraction of frames for which z(Cter) < 0 (during the 20−100 ns time range of the trajectories), and this is shown in Figure 6 for the studied amphiphiles. This figure also shows the expected fraction of interdigitated conformations, assuming that: (i) the NBD N1 atoms have transverse position equal to the average of those obtained from simulation of NBD-C_8, -C_{10}, -C_{12}, -C_{14}, and -C_{16}; (ii) the average transverse NBD N1-Cter distance varies linearly with n, with slope equal to that recovered from linear regression of all the values obtained from simulation (0.083 nm/CH_2); and (iii) the transverse position of the Cter atom follows a Gaussian distribution, with the average value calculated taking into account i and ii above, and a standard deviation equal to the average of the standard deviations (obtained from simulation) of the Cter z-coordinate of NBD-C_8, -C_{10}, -C_{12}, -C_{14}, and -C_{16}.

It can be seen that for $n \geq 10$ there is a sizable amount of simulation frames showing interdigitation of NBD-C_n, and for $n \geq 14$ interdigitation occurs during 50% or more of the analyzed time window. Because of the transverse location of the NBD fluorophore in the glycerol backbone/carbonyl region, it is not surprising that the longer chained amphiphiles are able to interdigitate. A similar effect was reported in the MD simulation of C_{18}-chained 1,1′-dioctadecyl-3,3,3′,3′-tetramethylindocarbocyanine (DiIC_{18}(3)), whose fluorophore has a similar transverse location to that of NBD, in fluid DPPC.[29] For interdigitation not to occur, the chains would have to present a higher amount of *gauche* defects, at an energetic cost. The fact that the variation of Cter<z> with n remains mostly linear and with a slope similar to that typical of fluid phospholipid acyl chains implies that this does not occur to a significant extent. In any case, Cter of the longer-chained derivative, NBD-C_{16}, is on average closer to the bilayer midplane than the terminal methyl groups of the POPC

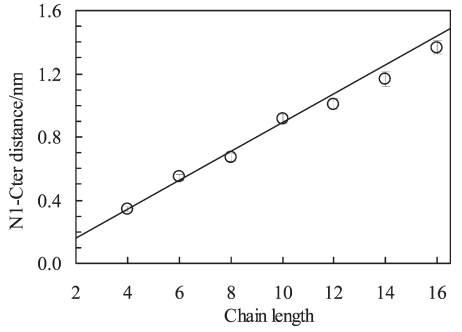

Figure 3. Variation of the transverse distance between N1 and the terminal methyl group of the amphiphiles (Cter). The line is the best linear fit to the $n \leq 10$ points, with a slope equal to 0.091 nm/CH_2.

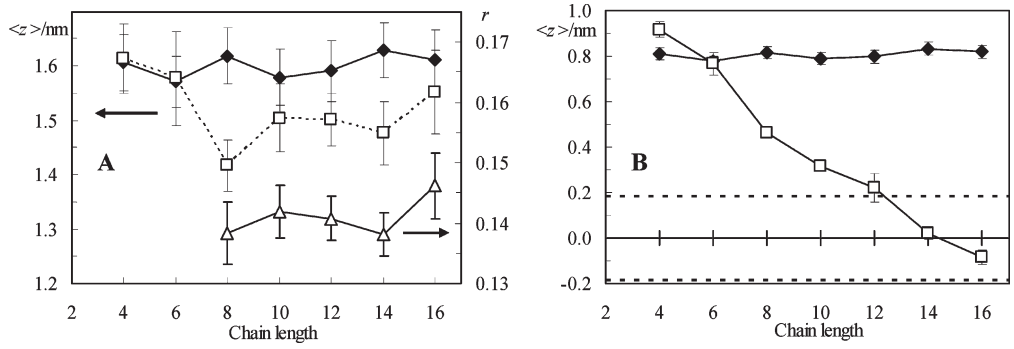

Figure 4. (A) Comparison between the average transverse positions <z> of C13 of POPC (black diamonds) and N6 of NBD-C_n (white squares). Also shown is the steady state fluorescence anisotropy (r) measured for $n \geq 8$ (white triangles).[1] (B) Comparison between average transverse positions of C24 of POPC (carbon 9 of the *sn*-2 chain; black diamonds) and the chain end methyl group (Cter; white squares) of NBD-C_n. The two dotted lines represent the average transverse location of the acyl chains' end methyl group in the two bilayer leaflets.

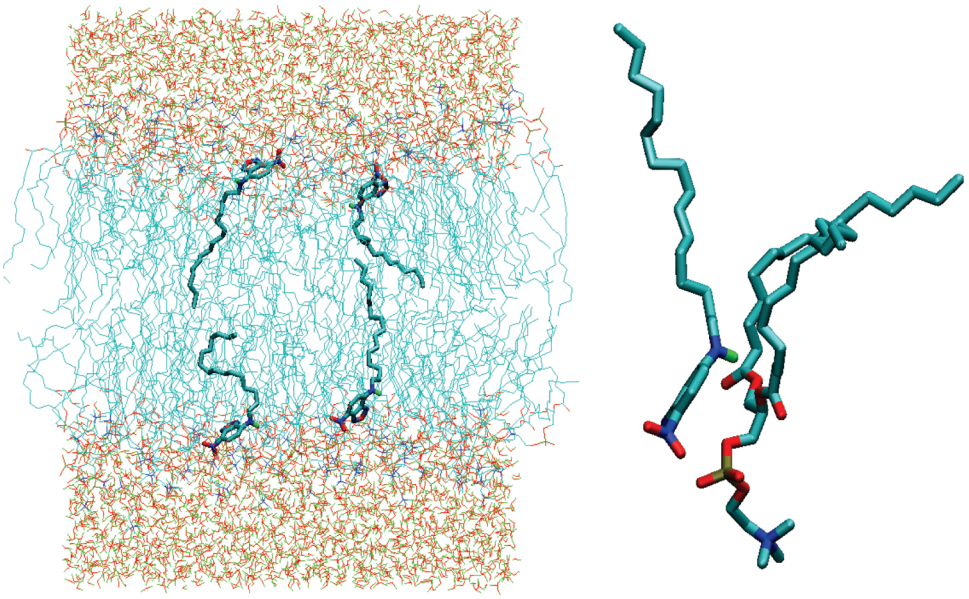

Figure 5. Left: typical snapshot of a POPC bilayer containing 4 NBD-C16 molecules, one of which displays clear interdigitation behavior. Right: zoomed snapshot of this interdigitating NBD-C_{16} and a nearby POPC molecule, showing NBD N1−NBD H14−POPC O14 hydrogen bonding. CH_n groups (n = 0−3), O atoms, N atoms, P atoms, and polar H atoms are displayed in cyan, red, blue, tan, and green, respectively.

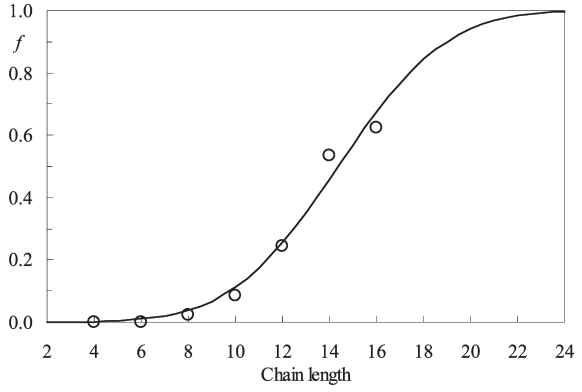

Figure 6. Fraction of interdigitated conformations (f) as a function of the amphiphile chain length n. The points are the values obtained from simulation, whereas the line was calculated assuming linear variation of <z>(Cter) and normal distribution of z(Cter) (see text for details).

molecules of the opposing leaflet (see Figure 4B), and the former remain thus located well within the highly disordered bilayer center. Probably, an even higher degree of interdigitation of NBD-C_{16}'s acyl chains (which, to some degree, could be anticipated from the calculated line shown in Figure 6) is not favored, which may also explain the relatively shallow location of the fluorophore for this analogue (Figure 4A). It is also noteworthy that NBD-C_{14} has a slightly lower Cter<z> than estimated from interpolation of the NBD-C_{12} and NBD-C_{16} values (Figure 4B) and also displays a somewhat higher degree of interdigitation than expected (Figure 6). This correlates with the slightly lower position of the fluorophore atoms observed for NBD-C_{14} compared to NBD-C_{10}, -C_{12}, and -C_{16} (Figure 4A) and is in line with experimental reports of a minimum in the activation enthalpy for the translocation process for NBD-C_{14}.[20] This experimental study also revealed a maximum in the entropic contribution for the activation Gibbs function of the desorption process of NBD-C_{12}, which could be explained taking into account that this probe is better accommodated within its bilayer leaflet than the others (because it stretches to the same extent as the host lipid chain, neither creating free space below it as the shorter chained amphiphiles, nor disturbing the opposite leaflet significantly, as the longer chained ones). On the other hand, the slightly deeper location of the fluorophore in NBD-C_{14} (into a less ordered region of the bilayer) agrees with a minimal value of average fluorescence anisotropy (despite the minimum in lifetime) observed for this amphiphile.[1] As seen in Figure 4A, fluorescence anisotropy also presents a minimum for NBD-C_8, following the trend observed in the <z> of NBD N6 calculated in this study. The variation of fluorescence quantum yield reported for $n \geq 8$ is also almost parallel to that of the calculated <z>.[1] Slight deviations (e.g., the average value of the quantum yield of NBD-C_8 is essentially identical—not clearly lower, as observed for NBD <z>—to those of NBD-C_{10} and NBD-C_{12}) probably reflect the increased uncertainty associated with the experimental determination of fluorescence quantum yield values in turbid media.

The physical reason for the deeper location of NBD-C_8 is not entirely clear although it is most likely a consequence of the position of Cter just below carbon 9 of the POPC acyl chain. Smaller alkyl chain amphiphiles are well-accommodated and located exclusively in the region of the POPC bilayer with properties of a soft polymer, while longer amphiphiles extend into the disordered region of the bilayer.[62,63] The location of the longer amphiphiles is therefore a balance between two forces: (i) maximization of the interactions with the lipids in the cavity around the amphiphile, which pulls the latter into the center of the bilayer, and (ii) maximization of the interactions between the polar portion of the amphiphile and the polar interface of the bilayer. Because the cavity below NBD-C_8 is larger than for longer amphiphiles, the first effect is expected to be maximal for this probe, leading to a deeper location.

Orientation of the NBD Fluorophore. Figure 7 shows the frequency distributions $P(\theta)$ of the angles between the long axis

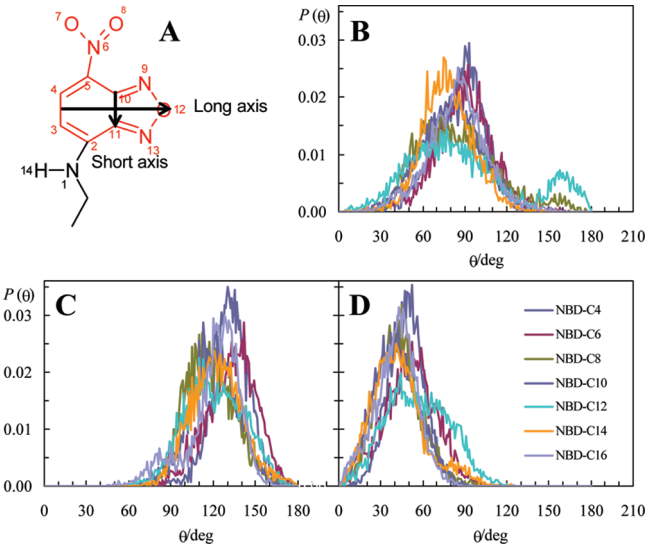

Figure 7. (A) Definition of long and short axes of the NBD fluorophore. (B–D) Probability density functions $P(\theta)$ of the angles between the long axis (B), the short axis (C), and the normal to the NBD plane (defined as the vector product of the short and long axes; D), relative to the bilayer normal.

(defined as the vector between atom O12 and the center of mass of atoms C3 and C4), the short axis (defined as the vector between atoms C10 and C11), and the normal to the NBD plane (defined as the vector product of the short and long axes) relative to the bilayer normal. For the short axis, similar $P(\theta)$ distributions are recovered for all systems. All distributions are wide, but values $\theta > 90°$ predominate clearly, corresponding to C_{10} being closer to the interface than C11. Given the rigidity of the NBD moiety, this is a necessary consequence of the higher $\langle z \rangle$ obtained for the NO_2 group compared to the remainder of the fluorophore, as illustrated above (Figures 2 and 5). For the long axis, $\theta \leq 90°$ predominates for all systems, corresponding to O12 being closer to the interface than the opposing end of this molecular axis. In any case, very similar $P(\theta)$ functions are obtained for the angle between the normal to the NBD plane and the bilayer normal.

Subtle variations in orientation correlate with differences in transverse position of the fluorophore. For example, NBD-C_4, -C_6, and C_{16} have short axis angle distributions shifted to higher values relative to the other molecules, in accordance with the more external placement of the N6 atom for these molecules (Figure 4A). This correlation, found both within each molecule's simulation run and across all systems, is evidenced in Figure S3 of the SI. In any case, on the whole, the preferred orientations of the NBD group in all systems are close to each other and similar to that of the same fluorophore in C12-NBD-PC in fluid DPPC bilayers.[30] This general orientation behavior, in which all electronegative O atoms (especially those of the $-NO_2$ group, O7 and O8, but also O12 in the ring system) point toward the water–lipid interface, is illustrated in the instant configurations of the left panel of Figure 5.

Hydrogen Bonding. The NBD fluorophore has an H atom bound to an amino N atom. This nitrogen can act as H-bond donor to water or POPC O atoms. On the other hand, there are several O and N atoms in the fluorophore, which can act as H-bond acceptors from water oxygen atoms. These interactions can be easily monitored in an MD simulation. For the following analysis, which used the last 80 ns of the simulations, an H-bond for a given donor–H–acceptor triad was registered each time the donor–acceptor distance was <0.35 nm and the H-donor–acceptor angle was <60°.

Figure 8A shows the frequency of H-bonding from NBD N1–H14 to each of the possible acceptor atoms. As can be readily seen by summing over all acceptors, the NBD NH group is almost continuously involved in H-bonds. Note that, because of the adopted definition of H-bonding, there can be more than one acceptor at the same time (if they are simultaneously located at a distance <0.35 nm to the NBD N1 atom and the H-donor–acceptor angle is <60° for both), and hence the totals can be higher than 100%. Low frequencies, in relative terms, are observed for all amphiphiles regarding H-bonding to water O atoms (except in the case of NBD-C_{12}) and to phosphate O atoms. In all cases, H-bonding is most common to O atoms within the glycerol backbone (O14 and O33) or to carbonyl O atoms (in the case of NBD-C_{12}, in which H-bonding to POPC O_{16} atoms was observed for ~17% of the frames). This behavior is identical to that reported for C12-NBD-PC[30] and correlates with the transverse location of the NBD group in the upper chain/glycerol region of the bilayer. In closer inspection, the H-donor–acceptor angle and the H-acceptor distance distributions reveal some degree of specificity. The preferred angle of the H-bond triad is below 20°, being ~15° for the case of the H-bond to O14. The almost perfect colinearity of the triad probably indicates preference of NBD N1–H14 for establishing H-bonds with this oxygen atom of POPC. This interaction is visible in the snapshot detail of Figure 5 (right panel).

The H-bonding between the –OH groups of water (donors) and the various O and N atoms of NBD (acceptors) shows preference for the O7 and O8 of the NBD (Figure 8B), in agreement with the higher exposure to the solvent by these two atoms and their significant negative charge ($\cong -0.5$ each[30]). Slight differences among amphiphiles can be correlated with other calculated properties. For example, NBD-C_8 has a short-axis angular distribution shifted to lower values in comparison to the other molecules (Figure 7). This implies that the NO_2 group protrudes less into the water/lipid interface and is probably reflected in the observed lower degree of H-bonding of this group to water (Figure 8B). On the other hand, both parts of Figure 7, A and B, show a slightly different behavior of NBD-C_{12}, which displays decreased H-bonding from NBD N1 to POPC O14, increased H-bonding from NBD N_1 to POPC O16 (Figure 8A), and increased H-bonding from water to NBD O7 (Figure 8B). This is probably related to the somewhat distinct orientation profiles of the NBD-C12 fluorophore (evident in the minor peak of the long axis angular profile at ~160°, see Figure 7B, and in the wider normal-to-NBD angular profile, Figure 7D). In any case, on detailed inspection, we found this to be due to the behavior of a single NBD-C12 molecule which equilibrates very slowly, maintaining an anomalous conformation for roughly the first half of the simulation run (not shown), rather than from a distinct behavior of NBD-C_{12} when compared to the other analogues.

As described above, in the NBD-C4, NBD-C6 and NBD-C8 simulations, one amphiphile molecule escaped the bilayer to the water medium. Whereas in the NBD-C4 system this molecule did not return to the bilayer during the simulation, for the other systems the escaping molecule (which was omitted from the results shown in Figure 8) re-entered the bilayer at a later stage of

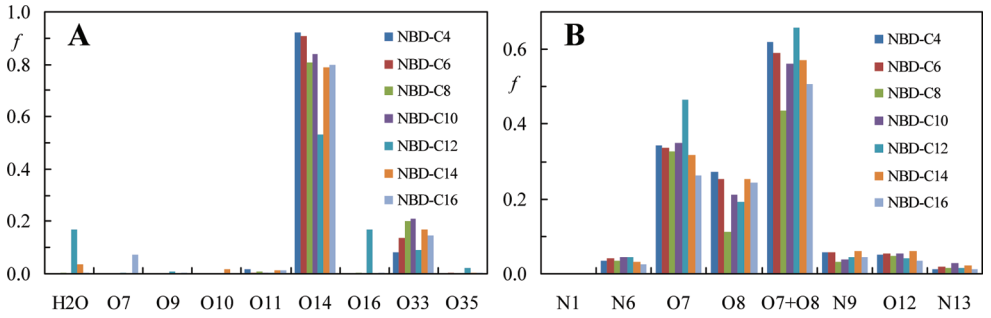

Figure 8. NBD N1−H14−POPC or water acceptor atom (A) and water donor−NBD acceptor atom (B) H-bond fractional frequencies (f).

the run, to a transverse location identical to the other three molecules. In the case of NBD-C_6, the returning amphiphile proceeds to establish H-bonding with POPC O14 and O33 atoms, similarly to the vast majority of molecules in all systems. In the case of NBD-C_8, however, the returning molecule goes on to establish H-bonds exclusively with the deeper O16 atoms of POPC. This difference illustrates the difficulty in obtaining complete equilibration when inserting amphiphiles from the water medium. These effects of amphiphile desorption and reentry in MD simulations are currently being studied in considerable detail by our group and will be addressed in a separate report. In any case, on the whole, these results indicate that the NBD-NH group preferably acts as H-bond donor to the ester O atom of the *sn*-2 acyl chain. This behavior was already apparent for the NBD fluorophore in C_{12}-NBD-PC in fluid DPPC bilayers.[30]

Order of the NBD-C_n and POPC Acyl Chains. In our simulations, using a united atom force field, deuterium order parameters (S_{CD}) for saturated (S_{CD}^{sat}) and unsaturated (S_{CD}^{unsat}) carbons are determined using the following relations:[64]

$$-S_{CD}^{sat} = \frac{2}{3}S_{xx} + \frac{1}{3}S_{yy} \quad (1)$$

$$-S_{CD}^{unsat} = \frac{1}{4}S_{zz} + \frac{3}{4}S_{yy} + \frac{\sqrt{3}}{2}S_{xy} \quad (2)$$

where S_{ab} are the order tensor coordinates, given by

$$S_{ab} = \frac{1}{2}\langle 3\cos\theta_a \, 3\cos\theta_b - \delta_{ab}\rangle \; a,b = x,y,z \quad (3)$$

where in turn θ_a (or θ_b) is the angle made by the ath (or bth) molecular axis with the bilayer normal and δ_{ab} is the Kronecker delta ($\langle\rangle$ denotes both ensemble and time averaging).

$-S_{CD}$ can vary between 0.5 (full order along the bilayer normal) and −0.25 (full order along the bilayer plane), whereas S_{CD} = 0 denotes isotropic orientation. Because of the slow convergence of this parameter,[63] the analysis was restricted to the last 50 ns of the simulations. Order parameters were calculated for both acyl chains of POPC (Figure S4 of the SI). For pure phospholipid bilayer, the profiles obtained agreed with both experimental (e.g.,[65,66]) and simulated (e.g.,[55,57,67,68]) data. Incorporation of NBD-C_n leads to nonmonotonic alterations, correlated with those of area/lipid discussed above (i.e., systems for which a higher a was obtained tend to present slightly lower $-S_{CD}$ profiles).

Focusing on the NBD-C_n chain order parameters, Figure 9A shows $-S_{CD}$ for the chain C atoms of the different amphiphiles. As expected, the order parameter decreases along the chain for each molecule, pointing to an increased fraction of *gauche* conformations near the end of the chain. However, a comparison of all systems together is rendered difficult due to poor statistics resulting from the low number of amphiphile molecules simulated in each run. To get further insight, we plotted the order parameter of each carbon segment as a function of the total number of carbons of the amphiphilic chain (Figure 9B). Two patterns may be identified from the plot: first, the order of each carbon segment generally increases with the total number of chain carbons. For every segment, the shorter-chained amphiphiles present lower $-S_{CD}$ values than the longer-chained amphiphiles. This is expected, because a higher number of carbons will induce a stronger anchoring effect of the amphiphiles in the bilayer for the same absolute position along the chain. Second, this increase is not smooth, and up to and including the C7 position along the chains local minima or maxima can be identified. For C2 and C3, these minima occur for NBD-C_8 and NBD-C_{14}, the amphiphiles for which the NBD atoms presented deeper penetration (Figure 2), implying a deeper location of the first carbon atoms of their chains, into a less ordered region of the bilayer. These two minima imply the existence of a maximum for an intermediate chain length (verified for n = 10) for these chain atoms. These features gradually vanish and can no longer be observed from the chain atom C8 onward.

Electrostatic Potential. Given the polarity of the NBD fluorophore, it can be expected beforehand that the incorporation of NBD-C_n in the bilayer affects the electrostatic profile. Figure 10 shows the potential at the center of the bilayer (relative to that in the water region) as a function of the number of chain carbons of the amphiphile. The value for pure POPC, −514 mV, agrees with recent MD studies, in which values ranging from −500 mV to −600 mV are reported.[55,68,69] The inclusion of the NBD-C_n amphiphiles increases the difference in electrostatic potential between the interior of the bilayer and the bulk water phase. These values are subject to uncertainty due to cancellation errors, because the observed potential profile is the difference between the water and lipid contributions, which almost cancel each other (not shown). In any case, the observed variation reflects in part the measured average area/lipid a. Systems with smaller a values (such as NBD-C_8 and -C_{14}, see Table 1) tend to present higher electrostatic potential in the membrane relative to the water medium (compatible with their higher average surface charge density) and conversely for systems with larger a (e.g., NBD-C_{10}). In any case, there is no doubt that the insertion of NBD-C_n amphiphiles increases the difference in electrostatic potential in the membrane relative to water. Similar effects were observed and discussed for the C_6-NBD-PC and C_{12}-NBD-PC probes.[27]

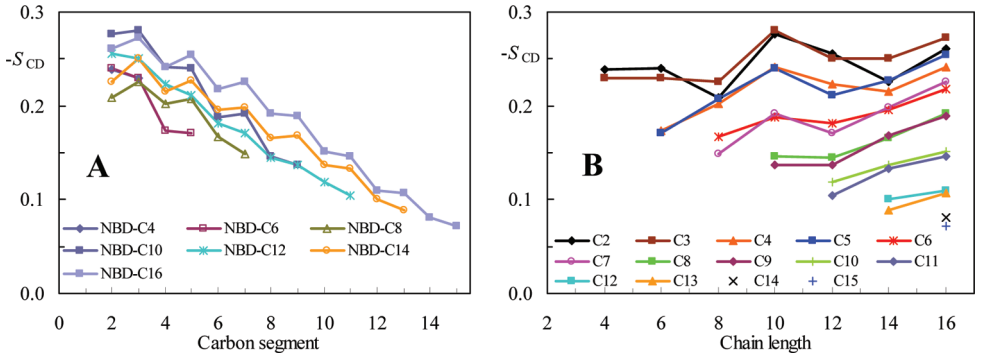

Figure 9. Deuterium order parameter of the NBD amphiphiles. (A) Perspective of the order of each amphiphile as a function of the carbon segment. (B) Perspective of the order of each carbon segment as a function of the number of total carbons of the amphiphilic chain.

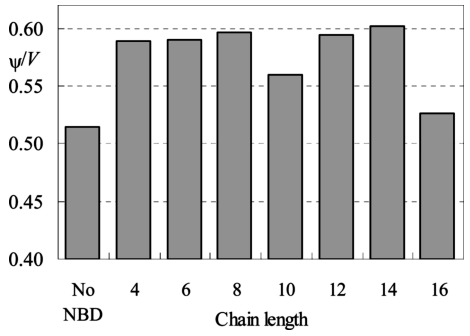

Figure 10. Electrostatic potential in the center of the bilayer (relative to the water region) as a function of the total number of carbons of the NBD-C_n amphiphilic chains.

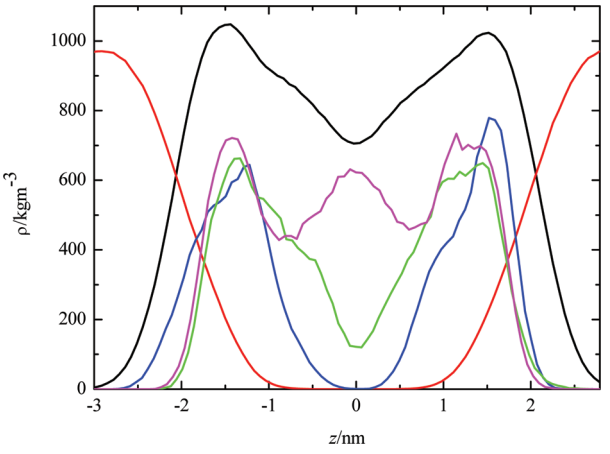

Figure 11. Mass density distributions of POPC (black) and water (red), both recovered from pure POPC bilayers, and NBD-C_6 (blue), -C_{10} (green), and -C_{16} (magenta), recovered from the respective 4 NBD-C_n/POPC systems. The profiles of the NBD amphiphiles were multiplied by 32 for better visualization.

Mass Density Profiles. Figure 11 shows the mass density profiles across the bilayer obtained for water, POPC, and selected (for clarity reasons) NBD-amphiphiles for the different POPC/NBD-C_n systems. To this effect, and because the bilayers' centers of mass may fluctuate in time, the positions of all atoms were determined relative to the instantaneous center of mass in all simulations, for each frame. Relative to pure POPC, alterations in the density profiles for water or POPC atoms in bilayers containing NBD-C_n are small and nonmonotonic (not shown), pointing to limited probe perturbation (already evidenced in the area/lipid and P−P distance results commented above). The most interesting result from this analysis is that an increase in the mass density at the center of the bilayer is observed for amphiphiles with alkyl chains longer than NBD-C_6. For the amphiphiles NBD-C_4 and NBD-C_6 the mass density profiles indicate that Cter does not reach the center of the bilayer, unlike for NBD-C_8 and NBD-C_{10}. For the amphiphiles with $n \geq 12$ there is a considerable increase in mass density, even presenting a local maximum, close to the bilayer center (unlike POPC itself). These results correlate with the fraction of interdigitated frames in each system (Figure 6), which becomes significant for $n \geq 12$.

Lateral Diffusion. Lateral diffusion coefficients of POPC in all systems were calculated from the two-dimensional mean square displacement (MSD), using the Einstein relation

$$D = \frac{1}{4} \lim_{t \to \infty} \frac{\mathrm{dMSD}(t)}{\mathrm{d}t} \tag{4}$$

In turn, MSD is defined by

$$\mathrm{MSD}(t) = \left\langle \left\| \vec{r}_i(t + t_0) - \vec{r}_i(t_0) \right\| \right\rangle^2 \tag{5}$$

where $\vec{r}_i$ is the (x,y) position of the center of mass of molecule i of a given species; the averaging is carried out over all molecules of this kind and time origins t_0. To eliminate noise due to fluctuations in the center of mass of each monolayer, all MSD analyses were carried out using trajectories with fixed center of mass of the corresponding monolayer,[48,70] and, to improve statistics, the final result was averaged over the two monolayers of all simulations carried out for each system.

Figure 12A shows the variation of lateral diffusion coefficient determined for POPC for systems labeled with the different amphiphiles. All calculated values are similar and close to that obtained for pure POPC, $(2.1 \pm 0.3) \times 10^{-8}$ $\mathrm{cm^2 s^{-1}}$, which in turn agrees well with values obtained both from NMR experiments[71,72] and MD simulations[55] ($1-4 \times 10^{-8}$ $\mathrm{cm^2 s^{-1}}$ for POPC near room temperature). The invariance of the calculated D upon the incorporation of these single-chained amphiphiles is another indicator of their relatively mild perturbation of the bilayer, in contrast with the NBD acyl-chain labeled PC.[27]

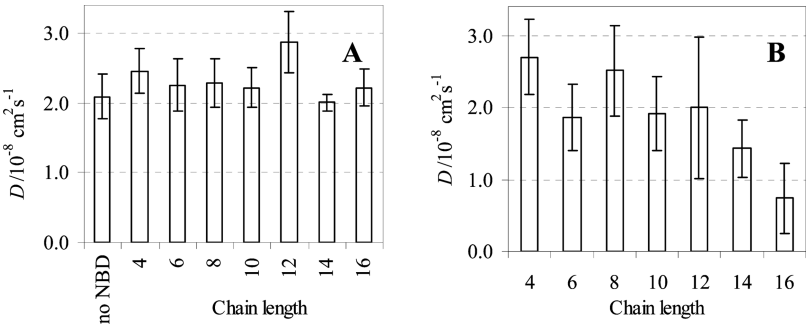

Figure 12. Diffusion coefficients of POPC (A) and NBD-C_n (B) for all studied systems.

Figure 12B shows the diffusion coefficients obtained for NBD-C_n. For $n \leq 12$, the calculated D values are similar to the corresponding values for POPC. A minimal average value is observed for NBD-C_6, though its difference relative to NBD-C_4 and NBD-C_8 is probably not significant. A decrease is observed from $n = 8$ onward, but for $n \leq 12$, D(NBD-C_n) is still statistically indistinguishable from that of POPC. Curiously, NBD-C_{12} is the amphiphile whose Cter is, on average, located at the same depth as the acyl-chain methyl groups of same-leaflet POPC molecules (Figures 2 and 4B). For NBD-C_{14} and NBD-C_{16}, the diffusion coefficient is clearly lower than that of POPC. This correlates with the increased degree of interdigitation observed for these amphiphiles' chains, and a probable cause of reduced lateral mobility is hindrance caused by the acyl chains of lipid molecules of the opposing bilayer leaflet.

CONCLUDING REMARKS

Atomistic MD simulations of POPC bilayers labeled with fluorescent fatty amines of varying alkyl chain length, NBD-C_n, were carried out. For the first time, a complete series of homologous fluorescent membrane probes is studied using MD simulations. It is likely that other commonly studied homologous series (such as fatty acid derivatives[6−13,15]) display many of the features unveiled by the present work. The results obtained for pure POPC in this work, as discussed throughout this paper, agree with both experimental and theoretical published data, and validate our choices for MD parameters.

We found that the NBD fluorophore is located near the glycerol backbone/carbonyl region of POPC for all derivatives. However, subtle differences in calculated parameters such as area per lipid, POPC deuterium order parameter, NBD-C_n chain order parameter (for the first atoms of each chain), and bilayer thickness (P−P distance) correlate with each other and also with the observed transverse location of the fluorophore. In turn, the variation of the latter parameter with probe chain length agrees well with small discrepancies measured in the photophysical properties of the various molecules. In particular, the slightly deeper location of the fluorophore in NBD-C_{14} agrees with lower fluorescence quantum yield and anisotropy measured for this amphiphile.[1] The location and orientation of the NBD fluorophore in this homologous series is similar to that determined for the acyl-chain labeled phospholipids C_6-NBD-PC and C_{12}-NBD-PC.[30] However, compared to the latter, the perturbation induced by moderate concentrations (up to 3.1 mol %) of NBD-C_n is relatively mild, as small, nonsystematic variations were observed for parameters such as average area per lipid, bilayer thickness, POPC order parameters, and the lateral diffusion coefficient. In C6-NBD-PC and C12-NBD-PC, the NBD group was observed to loop to a transverse location closer to the interface than to the center of the bilayer, thus creating a U-turn in the *sn*-2 chain of the probe, which explains the increased perturbation induced by these molecules.[27,30] This effect is absent in the NBD-C_n series. The longer chained NBD-C_n amphiphiles show significant mass density near the bilayer midplane, and the chains of these derivatives interdigitate to some extent the opposite bilayer leaflet. This phenomenon leads to a slower lateral diffusion for the longer-chained derivatives ($n > 12$). Amphiphiles with chain lengths inside the $8 \leq n \leq 12$ range have lateral diffusion coefficients similar to that of POPC and, also taking into account their relatively mild perturbing effect, are useful fluorescent reporters of bilayer dynamics. The same cannot be said for NBD-C_{14} and NBD-C_{16}, whose lateral diffusion coefficients are significantly lower than that of POPC (by a factor of ~3 for NBD-C_{16}). On the other hand, it was also observed that the shorter-chained amphiphiles ($n \leq 8$) are able to leave the bilayer and in some instances return during the course of a 100 ns MD run. Longer simulations of these systems are at the moment being carried out, to gain additional atomic-detailed mechanistic insight on the desorption and insertion of these amphiphiles in lipid bilayers.

The molecular details obtained by this work regarding the interaction of the NBD-C_n amphiphiles with the POPC lipid bilayer allow the rationalization of the nonmonotonic behavior obtained experimentally for the photophysical parameters of the amphiphiles and the kinetic and thermodynamic parameters for their interaction with the membranes: (i) the variation of the fluorescence quantum yield and anisotropy correlates with the location of the NBD group; (ii) the reduced dependence of the rate of NBD-C_n translocation with the increase in the length of the alkyl chain length for $n \geq 12$ correlates with the location of the terminal portion of the alkyl chain in the disordered region of the bilayer center; (iii) the maximal entropy variation obtained upon formation of the transition state in the desorption of NBD-C_{12} is due to the good structural matching between this amphiphile and the lipid bilayer, leading to the minimal entropy in the inserted state along the series.

ASSOCIATED CONTENT

Supporting Information. Time variation of area/lipid for all systems; correlation between short axis to bilayer normal angle and transverse position of fluorophore; POPC order parameter profiles. This material is available free of charge via the Internet at http://pubs.acs.org.

AUTHOR INFORMATION

Corresponding Author
*Telephone: +351 239488485. Fax: +351 239827126. E-mail: lloura@ff.uc.pt.

ACKNOWLEDGMENT

H.A.L.F. was supported by doctoral stipend No. SFRH/BD/65375/2009 by FCT, Fundação para a Ciência e a Tecnologia, Portugal. L.M.S.L. acknowledges funding by FEDER, through the COMPETE program, and by FCT, project reference FCOMP-01-0124-FEDER-010787 (FCT PTDC/QUI-QUI/098198/2008). M.J.M. acknowledges funding by FEDER, through the COMPETE program, and by FCT, project reference PTDC/QUI/64565/2006 and PTDC/QUI/68242/2006.

REFERENCES

(1) Cardoso, R. M. S.; Filipe, H. A. L.; Gomes, F.; Moreira, N. D.; Vaz, W. L. C.; Moreno, M. J. *J. Phys. Chem. B* **2010**, *114*, 16337–16346.
(2) Sampaio, J. L.; Moreno, M. J.; Vaz, W. L. C. *Biophys. J.* **2005**, *88*, 4064–4071.
(3) Estronca, L. M. B. B.; Moreno, M. J.; Vaz, W. L. C. *Biophys. J.* **2007**, *93*, 4244–4253.
(4) Estronca, L. M. B. B.; Moreno, M. J.; Laranjinha, J. A. N.; Almeida, L. M.; Vaz, W. L. C. *Biophys. J.* **2005**, *88*, 557–565.
(5) Abreu, M. S. C.; Moreno, M. J.; Vaz, W. L. C. *Biophys. J.* **2004**, *87*, 353–365.
(6) Pownall, H. J.; Hickson, D. L.; Smith, L. C. *J. Am. Chem. Soc.* **1983**, *105*, 2440–2445.
(7) Kleinfeld, A. M.; Storch, J. *Biochemistry* **1993**, *32*, 2053–2061.
(8) Peitzsch, R. M.; McLaughlin, S. *Biochemistry* **1993**, *32*, 10436–10443.
(9) Zhang, F. L.; Kamp, F.; Hamilton, J. A. *Biochemistry* **1996**, *35*, 16055–16060.
(10) Massey, J. B.; Bick, D. H.; Pownall, H. J. *Biophys. J.* **1997**, *72*, 1732–1743.
(11) Pool, C. T.; Thompson, T. E. *Biochemistry* **1998**, *37*, 10246–10255.
(12) Hoyrup, P.; Davidsen, J.; Jorgensen, K. *J. Phys. Chem. B* **2001**, *105*, 2649–2657.
(13) Thomas, R. M.; Baici, A.; Werder, M.; Schulthess, G.; Hauser, H. *Biochemistry* **2002**, *41*, 1591–1601.
(14) Fujikawa, M.; Ano, R.; Nakao, K.; Shimizu, R.; Akamatsu, M. *Bioorg. Med. Chem.* **2005**, *13*, 4721–4732.
(15) Resh, M. D. *Biochim. Biophys. Acta* **1999**, *1451*, 1–16.
(16) Nadolski, M. J.; Linder, M. E. *FEBS J.* **2007**, *274*, 5202–5210.
(17) Vogler, O.; Barcelo, J. M.; Ribas, C.; Escriba, P. V. *Biochim. Biophys. Acta* **2008**, *1778*, 1640–1652.
(18) Martins, P. A.; Gomes, F.; Vaz, W. L. C.; Moreno, M. J. *Biochim. Biophys. Acta* **2008**, *1778*, 1308–1315.
(19) Chattopadhyay, A. *Chem. Phys. Lipids* **1990**, *53*, 1–15.
(20) Cardoso, R. M. S.; Martins, P. A.; Gomes, F.; Doktorovova, S.; Vaz, W. L. C.; Moreno, M. J. *J. Phys. Chem. B* **2011**DOI: 10.1021/jp203429s.
(21) Lakowicz, J. R. *Principles of Fluorescence Spectroscopy*, 3rd ed.; Springer: New York, 2006.
(22) Marrink, S. J.; de Vries, A. H.; Tieleman, D. P. *Biochim. Biophys. Acta* **2009**, *1788*, 149–168.
(23) Loura, L. M. S.; Carvalho, A. J. P.; Ramalho, J. P. P. *J. Mol. Struct.: THEOCHEM* **2010**, *946*, 107–112.
(24) Kyrychenko, A. *Chem. Phys. Lett.* **2010**, *485*, 95–99.
(25) Franova, M.; Repakova, J.; Capkova, P.; Holopainen, J. M.; Vattulainen, I. *J. Phys. Chem. B* **2010**, *114*, 2704–2711.
(26) Skaug, M. J.; Longo, M. L.; Faller, R. *J. Phys. Chem. B* **2009**, *113*, 8758–8766.
(27) Loura, L. M. S.; Fernandes, F.; Fernandes, A. C.; Ramalho, J. P. P. *Biochim. Biophys. Acta* **2008**, *1778*, 491–501.
(28) Holtta-Vuori, M.; Uronen, R. L.; Repakova, J.; Salonen, E.; Vattulainen, I.; Panula, P.; Li, Z. G.; Bittman, R.; Ikonen, E. *Traffic* **2008**, *9*, 1839–1849.
(29) Gullapalli, R. R.; Demirel, M. C.; Butler, P. J. *Phys. Chem. Chem. Phys.* **2008**, *10*, 3548–3560.
(30) Loura, L. M. S.; Ramalho, J. P. P. *Biochim. Biophys. Acta* **2007**, *1768*, 467–478.
(31) Curdova, J.; Capkova, P.; Plasek, J.; Repakova, J.; Vattulainen, I. *J. Phys. Chem. B* **2007**, *111*, 3640–3650.
(32) Repakova, J.; Holopainen, J. M.; Karttunen, M.; Vattulainen, I. *J. Phys. Chem. B* **2006**, *110*, 15403–15410.
(33) Repakova, J.; Holopainen, J. M.; Morrow, M. R.; McDonald, M. C.; Capkova, P.; Vattulainen, I. *Biophys. J.* **2005**, *88*, 3398–3410.
(34) Hoff, B.; Strandberg, E.; Ulrich, A. S.; Tieleman, D. P.; Posten, C. *Biophys. J.* **2005**, *88*, 1818–1827.
(35) Repakova, J.; Capkova, P.; Holopainen, J. M.; Vattulainen, I. *J. Phys. Chem. B* **2004**, *108*, 13438–13448.
(36) Lindahl, E.; Hess, B.; van der Spoel, D. *J. Mol. Model.* **2001**, *7*, 306–317.
(37) Berendsen, H. J. C.; Vanderspoel, D.; Vandrunen, R. *Comput. Phys. Commun.* **1995**, *91*, 43–56.
(38) Berendsen, H. J. C.; Postma, J. P. M.; Van Gunsteren, W. F.; Hermans, J. In *Intermolecular Forces*; Pullman, B., Ed.; Reidl: Dordrecht, The Netherlands, 1981; pp 331−342.
(39) Berger, O.; Edholm, O.; Jahnig, F. *Biophys. J.* **1997**, *72*, 2002–2013.
(40) Schuttelkopf, A. W.; van Aalten, D. M. F. *Acta Crystallogr., Sect. D: Biol. Crystallogr.* **2004**, *60*, 1355–1363.
(41) Schmidt, M. W.; Baldridge, K. K.; Boatz, J. A.; Elbert, S. T.; Gordon, M. S.; Jensen, J. H.; Koseki, S.; Matsunaga, N.; Nguyen, K. A.; Su, S. J.; Windus, T. L.; Dupuis, M.; Montgomery, J. A. *J. Comput. Chem.* **1993**, *14*, 1347–1363.
(42) Gordon, M. S.; Schmidt, M. W. *Advances in Electronic Structure Theory: GAMESS a Decade Later*; Elsevier: Amsterdam, 2005.
(43) Jorgensen, W. L.; Maxwell, D. S.; TiradoRives, J. *J. Am. Chem. Soc.* **1996**, *118*, 11225–11236.
(44) Besler, B. H.; Merz, K. M.; Kollman, P. A. *J. Comput. Chem.* **1990**, *11*, 431–439.
(45) Miyamoto, S.; Kollman, P. A. *J. Comput. Chem.* **1992**, *13*, 952–962.
(46) Hess, B.; Bekker, H.; Berendsen, H. J. C.; Fraaije, J. *J. Comput. Chem.* **1997**, *18*, 1463–1472.
(47) Feenstra, K. A.; Hess, B.; Berendsen, H. J. C. *J. Comput. Chem.* **1999**, *20*, 786–798.
(48) Anezo, C.; de Vries, A. H.; Holtje, H. D.; Tieleman, D. P.; Marrink, S. J. *J. Phys. Chem. B* **2003**, *107*, 9424–9433.
(49) Berendsen, H. J. C.; Postma, J. P. M.; Vangunsteren, W. F.; Dinola, A.; Haak, J. R. *J. Chem. Phys.* **1984**, *81*, 3684–3690.
(50) Essmann, U.; Perera, L.; Berkowitz, M. L.; Darden, T.; Lee, H.; Pedersen, L. G. *J. Chem. Phys.* **1995**, *103*, 8577–8593.
(51) Flyvbjerg, H.; Petersen, H. G. *J. Chem. Phys.* **1989**, *91*, 461–466.
(52) Lantzsch, G.; Binder, H.; Heerklotz, H.; Wendling, M.; Klose, G. *Biophys. Chem.* **1996**, *58*, 289–302.
(53) Konig, B.; Dietrich, U.; Klose, G. *Langmuir* **1997**, *13*, 525–532.
(54) Smaby, J. M.; Momsen, M. M.; Brockman, H. L.; Brown, R. E. *Biophys. J.* **1997**, *73*, 1492–1505.
(55) Bockmann, R. A.; Hac, A.; Heimburg, T.; Grubmuller, H. *Biophys. J.* **2003**, *85*, 1647–1655.
(56) Mukhopadhyay, P.; Vogel, H. J.; Tieleman, D. P. *Biophys. J.* **2004**, *86*, 337–345.
(57) Gurtovenko, A. A.; Anwar, J. *J. Phys. Chem. B* **2009**, *113*, 1983–1992.
(58) Pandit, S. A.; Chiu, S. W.; Jakobsson, E.; Grama, A.; Scott, H. L. *Langmuir* **2008**, *24*, 6858–6865.
(59) Raghuraman, H.; Shrivastava, S.; Chattopadhyay, A. *Biochim. Biophys. Acta* **2007**, *1768*, 1258–1267.

(60) Huster, D.; Muller, P.; Arnold, K.; Herrmann, A. *Biophys. J.* **2001**, *80*, 822–831.
(61) Cevc, G.; Marsh, D. *Phospholipid Bilayers. Physical Principles and Models*; John Wiley & Sons: New York, 1987.
(62) Bemporad, D.; Essex, J. W.; Luttmann, C. *J. Phys. Chem. B* **2004**, *108*, 4875–4884.
(63) Tieleman, D. P.; Marrink, S. J.; Berendsen, H. J. C. *Biochim. Biophys. Acta* **1997**, *1331*, 235–270.
(64) Douliez, J. P.; Leonard, A.; Dufourc, E. J. *Biophys. J.* **1995**, *68*, 1727–1739.
(65) Klose, G.; Madler, B.; Schafer, H.; Schneider, K. P. *J. Phys. Chem. B* **1999**, *103*, 3022–3029.
(66) Seelig, J.; Waespesarcevic, N. *Biochemistry* **1978**, *17*, 3310–3315.
(67) Klauda, J. B.; Venable, R. M.; Freites, J. A.; O'Connor, J. W.; Tobias, D. J.; Mondragon-Ramirez, C.; Vorobyov, I.; MacKerell, A. D.; Pastor, R. W. *J. Phys. Chem. B* **2010**, *114*, 7830–7843.
(68) Patra, M.; Salonen, E.; Terama, E.; Vattulainen, I.; Faller, R.; Lee, B. W.; Holopainen, J.; Karttunen, M. *Biophys. J.* **2006**, *90*, 1121–1135.
(69) Gurtovenko, A. A.; Vattulainen, I. *J. Chem. Phys.* **2009**, 130.
(70) Lindahl, E.; Edholm, O. *J. Chem. Phys.* **2001**, *115*, 4938–4950.
(71) Febo-Ayala, W.; Holland, D. P.; Bradley, S. A.; Thompson, D. H. *Langmuir* **2007**, *23*, 6276–6280.
(72) Kochy, T.; Bayerl, T. M. *Phys. Rev. E* **1993**, *47*, 2109–2116.